

Bianisotropy for light trapping in all-dielectric metasurfacesAndrey B. Evlyukhin^{1,*}, Vladimir R. Tuz^{2,†}, Valentyn S. Volkov,³ and Boris N. Chichkov^{1,4}¹*Institute of Quantum Optics, Leibniz Universität Hannover, Welfengarten Street 1, 30167 Hannover, Germany*²*State Key Laboratory of Integrated Optoelectronics, College of Electronic Science and Engineering, International Center of Future Science, Jilin University, 2699 Qianjin Street, Changchun 130012, China*³*Moscow Institute of Physics and Technology, 9 Institutsky Lane, Dolgoprudny 141700, Russia*⁴*Lebedev Physical Institute, Leninsky Prospekt 53, 119333 Moscow, Russia*

(Received 11 February 2020; revised manuscript received 22 April 2020; accepted 23 April 2020; published 13 May 2020)

Magnetolectric dipole coupling effects in all-dielectric metasurfaces composed of particles with bianisotropic electromagnetic response are investigated. This bianisotropic response is associated with the trapped mode excitation. Maintaining the trapped mode resonant conditions allows one to sufficiently increase the quality factor and reduce radiation losses in all-dielectric nanostructures (metasurfaces). An analytical model accounting for the contributions of both electric and magnetic dipole moments induced in particles by external electromagnetic fields is proposed. We show how bianisotropy can lead to the excitation of the trapped mode in metasurfaces. This mode corresponds to the electromagnetic coupling between the out-of-plane particle dipole moments, which do not radiate collectively from the metasurface plane resulting in the enhanced storage of electromagnetic energy. Our approach reveals a physical mechanism of the trapped mode excitation and demonstrates that the specially initiated bianisotropy of particles enables the energy flow between external electromagnetic waves and the trapped mode. Due to this bianisotropy, one can control the process of light-matter interaction and energy storage in all-dielectric metasurfaces via excitation of trapped modes.

DOI: [10.1103/PhysRevB.101.205415](https://doi.org/10.1103/PhysRevB.101.205415)**I. INTRODUCTION**

All-dielectric nanostructures are promising for use in advanced optoelectronics devices [1]. Such nanostructures can be fabricated from a wide range of dielectric and semiconductor materials (e.g., silicon) utilizing laser-assisted techniques [2] or standard nanolithography and complementary metal-oxide-semiconductor (CMOS) technologies [3]. Compatibility with the CMOS technologies is the major advantage of all-dielectric nanostructures over metallic (plasmonic) nanoparticle systems [4].

Typically, all-dielectric nanostructures are composed of a set of subwavelength particles made of materials with high or moderate refractive indexes [5,6]. At optical frequencies, particles support many electric and magnetic resonances [7–9] (often referred to as Mie resonances [10]), which arise due to light field penetration inside the particles and resonant excitation of their polarization currents. Therefore, each particle in the structure behaves as an individual nanoresonator, whereas their collective response determines the resonant characteristics of the entire all-dielectric nanostructure.

Since the Mie resonances are accompanied by a strong enhancement of electromagnetic field inside the high-refractive-index nanoparticles [2,11], the current trend in the field of all-dielectric nanostructures is associated with their application in nonlinear optics [12–15]. It is revealed [16,17] that efficiencies of nonlinear optical processes in all-dielectric

nanostructures can be very high exceeding by several orders corresponding characteristics achieved in plasmonic nanoparticle systems [18,19]. Moreover, the efficiency of light-matter interactions in dielectric nanostructures can be substantially enhanced by increasing the quality factor of individual nanoresonators forming the system, while providing their low overhead absorption and radiation losses. This is achieved by choosing a special form of dielectric nanoresonators, which are made of low-loss materials.

An effective way to reduce radiation losses and increase the quality factor of resonances in all-dielectric nanostructures is to maintain excitations related to the so-called trapped modes [20]. The trapped modes can be excited in all-dielectric nanostructures if their constitutive resonators are in some way perturbed [21–23]. A perturbation transforms inherently nonradiative (dark) modes to weakly radiative ones when spatial symmetry of the unit cell of the nanoparticle system is broken. Recently, the excitation of trapped modes in such asymmetrical structures was discussed in the framework of the concept of symmetry-protected bound states in the continuum (BICs) [24–27].

In the framework of BICs, the existence of trapped modes in all-dielectric metasurfaces composed of perturbed disks has been recently studied both numerically and experimentally [28–31]. It has been proven that in such metasurfaces, the trapped modes can be excited under normal plane wave incidence conditions. The excitation of trapped modes leads to a strong near-field enhancement, which may initiate the nonlinear [30] and thermal [31] processes in the nanostructure. The reported numerical and experimental results convincingly

* a.b.evlyukhin@daad-alumni.de

† tvr@jlu.edu.cn

demonstrate the practical importance of the effect of trapped modes in all-dielectric nanostructures.

The excitation of trapped modes leads to arising narrow Fano resonances in the spectral characteristics of metasurfaces. This effect is similar to the excitation of surface lattice resonances (SLRs) in one-dimensional (1D) [32–34] and two-dimensional (2D) [7,35,36] structures composed of periodic arrays of dipole nanoparticles (see a comprehensive review on SLRs in plasmonic arrays in Ref. [37]). In both cases, the Fano resonances arise owing to a general mechanism related to the coupling between a broadband bright mode and a narrow-band dark mode supported by a system [38]. However, there is an important difference between the trapped modes and SLRs. The SLRs are diffraction resonances determined by the ratio on the wavelength and the period of the structure. They originate from the transition of a diffractive order from a propagating state into an evanescent state in the area of the Rayleigh anomaly. However, the trapped mode can exist under the long-wavelength conditions without the diffraction assistance. They are deep subwavelength resonances whose excitation requires a special design of spatially asymmetric unit cells.

Since all-dielectric nanostructures are composed of sub-wavelength particles, their optical properties are related to resonant features of individual resonators and their mutual interactions. In most cases, especially for particles having a simple form, only electric and magnetic dipole contributions are significant, and their proper accounting allows one to adequately describe characteristics of the nanostructure in the coupled dipole approximation [7,39,40]. Such a description can be expressed in terms of polarizabilities, which define the linear relations between dipole moments induced in a single resonator by external electromagnetic fields [41,42]. Ordinary, this approach assumes that electric and magnetic dipole moments of each particle in the nanostructure are excited independently by the electric and magnetic field components of the incident wave, respectively. However, in all-dielectric nanostructures supporting the trapped modes, particles can have a rather complicated shape [43–46]. In such particles, as it will be shown in this paper, in addition to direct electric and magnetic dipole response, a bianisotropic response can occur due to magnetoelectric coupling. This magnetoelectric coupling enables the excitation of magnetic dipoles by an electric field and of electric dipoles by a magnetic field. Therefore, the bianisotropic properties of a single particle are responsible for the collective bianisotropy of their ensemble [47–50]. The signature of the effect of bianisotropy appears in the constitutive relations, where the dependence of electrical induction on the magnetic field and magnetic induction on the electric field is expressed in the corresponding cross-polarizability terms [51].

In this paper, we show the correspondence between the resonant bianisotropic properties of a single particle and the conditions of resonant trapped mode excitation in an all-dielectric metasurface composed of such particles and irradiated by a normally incident electromagnetic wave. This effect leads to the high-quality-factor resonances in the metasurface reflection and transmission spectra. For our aims, we first develop the coupled dipole approximation (the coupled dipole equation method), which involves bianisotropy terms and then apply this method for studying electromagnetic properties of

the realistic all-dielectric metasurface. Since the bianisotropy of the nanoparticles allows an energy flow between external electromagnetic waves and the trapped mode in the metasurface, one can consider this mode as a quasi-trapped mode, the lifetime of which is determined by the radiation losses.

To construct a metasurface supporting trapped modes, here we employ a set of identical subwavelength high-refractive-index dielectric particles made in the form of a disk. To gain access to the trapped mode of the metasurface, the in-plane symmetry of the resonators is broken provided that each disk is perturbed by an eccentric through hole. Breaking symmetry of the disk resonator causes the existence of bianisotropy, which is also a subject of our subsequent study. The particle polarizability tensors are calculated numerically applying the method proposed in Refs. [41,42]. Total induced electric polarization current inside the particles and their electric and magnetic dipole moments are derived using the discrete dipole approximation [52] and approach developed earlier in Refs. [53,54]. Importantly, in this paper, we consider monochromatic time dependence $\exp(-i\omega t)$ for all corresponding values (ω is the angular frequency). For compactness, this explicit time dependence is accepted and omitted in this paper.

The rest of the paper is organized as follows. Section II presents a general theoretical background based on the coupled dipole equations including bianisotropy terms for arbitrary finite and infinite arrays of dielectric nanoparticles. Then, for an infinite 2D periodic array (metasurface) of identical nanoparticles, a formal solution is derived. In Sec. III we reveal the electromagnetic properties of an individual nanodisk and derive its dyadic polarizabilities. Then, the problem of light trapping in a metasurface composed of such nanodisks is investigated in detail. In particular, we show that the trapped mode is associated with the coupling between the out-of-plane particle dipole moments, which do not radiate collectively from the metasurface plane. The main results are summarized, and the conclusions are offered in Sec. IV.

II. THEORETICAL BACKGROUND

A. Coupled dipole model accounting for bianisotropy

In the dipole approximation, each nanoparticle in the particles' array is substituted by point electric and magnetic dipoles. Taking into account the effect of bianisotropy, the vectors of the electric \mathbf{p}_l and magnetic \mathbf{m}_l dipole moments of a particle with number l disposed at the position \mathbf{r}_l are determined by the relations between the external local electric $\mathbf{E}^{\text{loc}}(\mathbf{r}_l)$ and local magnetic $\mathbf{H}^{\text{loc}}(\mathbf{r}_l)$ fields [51]:

$$\begin{aligned}\mathbf{p}_l &= \hat{\alpha}_l^{\text{ee}} \mathbf{D}^{\text{loc}}(\mathbf{r}_l) + c_d^{-1} \hat{\alpha}_l^{\text{em}} \mathbf{H}^{\text{loc}}(\mathbf{r}_l), \\ \mathbf{m}_l &= \hat{\alpha}_l^{\text{mm}} \mathbf{H}^{\text{loc}}(\mathbf{r}_l) + c_d \hat{\alpha}_l^{\text{me}} \mathbf{D}^{\text{loc}}(\mathbf{r}_l),\end{aligned}\quad (1)$$

where $\hat{\alpha}_l^{\text{ee}}$, $\hat{\alpha}_l^{\text{mm}}$, $\hat{\alpha}_l^{\text{em}}$, and $\hat{\alpha}_l^{\text{me}}$ are four (electric, magnetic, electromagnetic, and magnetoelectric) dyadic polarizabilities related to the particle with number l , $\mathbf{D}^{\text{loc}}(\mathbf{r}_l) = \varepsilon_0 \varepsilon_d \mathbf{E}^{\text{loc}}(\mathbf{r}_l)$ is the local displacement field, and $c_d = (\mu_0 \varepsilon_0 \varepsilon_d)^{-1/2}$ is the light speed in homogeneous ambient space with relative permittivity ε_d . Here ε_0 and μ_0 are the vacuum permittivity and permeability, respectively. Generally, the polarizabilities comprise $4 \times 9 = 36$ polarizability components.

Note, for the cross polarizabilities, the condition $\hat{\alpha}^{\text{em}} = (-\hat{\alpha}^{\text{me}})^T$ holds from the time-reversal symmetry of the Maxwell's equations and linearity of the particle response [51,55–57] (here T denotes the transpose operation).

The local fields acting on the particle with number l are induced by both external incident waves with the fields $\mathbf{D}(\mathbf{r}_l) =$

$\varepsilon_0 \varepsilon_d \mathbf{E}(\mathbf{r}_l) = \varepsilon_0 \varepsilon_d \mathbf{E} \exp(i\mathbf{k}_d \mathbf{r}_l)$ and $\mathbf{H}(\mathbf{r}_l) = \mathbf{H} \exp(i\mathbf{k}_d \mathbf{r}_l)$, and the dipole moments of all other nanoparticles (with number $j \neq l$) forming the array. Using expressions from Refs. [7,58] for electric and magnetic fields generated by electric and magnetic dipoles, Eq. (1) for calculation of the dipole moments of all particles can be represented as

$$\begin{aligned} \mathbf{p}_l &= \hat{\alpha}_l^{\text{ee}} \left[\mathbf{D}(\mathbf{r}_l) + k_d^2 \sum_{j=1, j \neq l}^N \left(\hat{G}_{lj} \mathbf{p}_j + \frac{i}{k_d c_d} [\mathbf{g}_{lj} \times \mathbf{m}_j] \right) \right] + c_d^{-1} \hat{\alpha}_l^{\text{em}} \left[\mathbf{H}(\mathbf{r}_l) + k_d^2 \sum_{j=1, j \neq l}^N \left(\hat{G}_{lj} \mathbf{m}_j - \frac{i c_d}{k_d} [\mathbf{g}_{lj} \times \mathbf{p}_j] \right) \right], \\ \mathbf{m}_l &= \hat{\alpha}_l^{\text{mm}} \left[\mathbf{H}(\mathbf{r}_l) + k_d^2 \sum_{j=1, j \neq l}^N \left(\hat{G}_{lj} \mathbf{m}_j - \frac{i c_d}{k_d} [\mathbf{g}_{lj} \times \mathbf{p}_j] \right) \right] + c_d \hat{\alpha}_l^{\text{me}} \left[\mathbf{D}(\mathbf{r}_l) + k_d^2 \sum_{j=1, j \neq l}^N \left(\hat{G}_{lj} \mathbf{p}_j + \frac{i}{k_d c_d} [\mathbf{g}_{lj} \times \mathbf{m}_j] \right) \right], \end{aligned} \quad (2)$$

where $l = 1, 2, 3, \dots, N$, $k_d = |\mathbf{k}_d| = |\mathbf{k}| \sqrt{\varepsilon_d}$ is the wave number in the medium with ε_d , \mathbf{k} is the wave vector in vacuum, and $\hat{G}_{lj} = \hat{G}(\mathbf{r}_l, \mathbf{r}_j)$ and $\mathbf{g}_{lj} = \mathbf{g}(\mathbf{r}_l, \mathbf{r}_j)$ are the Green's functions (see Eqs. (2) and (3) in Ref. [7]).

After solving system (2) for an array composed of N nanoparticles, one can calculate in the dipole approximation the extinction power P_{ext} and scattered power P_{sca} [7,58]

$$P_{\text{ext}} = \frac{\omega}{2} \text{Im} \sum_{l=1}^N \{ \mathbf{E}^*(\mathbf{r}_l) \cdot \mathbf{p}_l + \mu_0 \mathbf{H}^*(\mathbf{r}_l) \cdot \mathbf{m}_l \}, \quad (3)$$

$$P_{\text{sca}} = \frac{1}{32\pi^2} \sqrt{\frac{\varepsilon_0 \varepsilon_d}{\mu_0}} \frac{k_0^4}{\varepsilon_0^2} \int \left| \sum_{l=1}^N e^{-ik_d(\mathbf{n} \cdot \mathbf{r}_l)} \left\{ \mathbf{n} \times [\mathbf{p}_l \times \mathbf{n}] + \frac{1}{c_d} [\mathbf{m}_l \times \mathbf{n}] \right\} \right|^2 d\Omega, \quad (4)$$

where the asterisk $*$ denotes complex conjugation, $\mathbf{n} = \mathbf{r}/|\mathbf{r}| = (\sin \theta \cos \phi, \sin \theta \sin \phi, \cos \theta)$ is the unit vector determining the scattering direction, $d\Omega = \sin \theta d\phi d\theta$ is the element of the solid angle Ω , and θ and ϕ are the polar and azimuthal angles of the spherical coordinate system, respectively. Integration in Eq. (4) is performed over the full solid angle.

The origin of the corresponding Cartesian coordinate system is chosen inside the region occupied by the array of nanoparticles. Total electric and magnetic fields at any point \mathbf{r} outside the array are a superposition of the fields of incident waves and the fields radiated by all electric and magnetic dipoles related to the nanoparticles. These total fields are

$$\begin{aligned} \mathbf{E}_{\text{tot}}(\mathbf{r}) &= \mathbf{E}(\mathbf{r}) + \frac{k_d^2}{\varepsilon_0 \varepsilon_d} \sum_{l=1}^N \left(\hat{G}_l \mathbf{p}_l + \frac{i}{k_d c_d} [\mathbf{g}_l \times \mathbf{m}_l] \right), \\ \mathbf{H}_{\text{tot}}(\mathbf{r}) &= \mathbf{H}(\mathbf{r}) + k_d^2 \sum_{l=1}^N \left(\hat{G}_l \mathbf{m}_l - \frac{i c_d}{k_d} [\mathbf{g}_l \times \mathbf{p}_l] \right), \end{aligned} \quad (5)$$

where $\hat{G}_l = \hat{G}(\mathbf{r}, \mathbf{r}_l)$ and $\mathbf{g}_l = \mathbf{g}(\mathbf{r}, \mathbf{r}_l)$. Since the extinction and scattering powers are parametrically dependent on the introduced polarizabilities, they take into account bianisotropy of the entire nanoparticle array. This method can be applied to both a finite and an infinite array of particles.

B. Infinite 2D periodic array of identical particles

Here we consider the general case of a plane electromagnetic wave interacting with an infinite 2D periodic array of

identical nanoparticles possessing bianisotropy. Under normal incidence conditions of an external plane electromagnetic wave, all particles forming the array bear the same electric \mathbf{p} and magnetic \mathbf{m} dipole moments. Using the approach developed in Ref. [7], generalized system of equations (2) is transformed to

$$\begin{aligned} \mathbf{p} &= \hat{\alpha}^{\text{ee}} [\mathbf{D} + k_d^2 \hat{G}^0 \mathbf{p}] + c_d^{-1} \hat{\alpha}^{\text{em}} [\mathbf{H} + k_d^2 \hat{G}^0 \mathbf{m}], \\ \mathbf{m} &= \hat{\alpha}^{\text{mm}} [\mathbf{H} + k_d^2 \hat{G}^0 \mathbf{m}] + c_d \hat{\alpha}^{\text{me}} [\mathbf{D} + k_d^2 \hat{G}^0 \mathbf{p}], \end{aligned} \quad (6)$$

where $\mathbf{D} = \varepsilon_0 \varepsilon_d \mathbf{E}$ and \mathbf{H} are the fields of the incident wave at the array plane, and equation

$$\hat{G}^0 = \sum_{j=2}^{\infty} \hat{G}(0, \mathbf{r}_j) \quad (7)$$

is the dipole sum tensor (here we assume that the nanoparticle with number $j = 1$ is disposed at the origin of chosen Cartesian coordinate system, so $\mathbf{r}_1 = 0$). A formal solution of system (6) can be written in the following form:

$$\begin{aligned} \mathbf{p} &= \hat{A}^{-1} [\hat{\alpha}^{\text{ee}} + k_d^2 \hat{\alpha}^{\text{em}} \hat{G}^0 (\hat{U} - k_d^2 \hat{\alpha}^{\text{mm}} \hat{G}^0)^{-1} \hat{\alpha}^{\text{me}}] \mathbf{D} \\ &\quad + \hat{A}^{-1} c_d^{-1} \hat{\alpha}^{\text{em}} [\hat{U} + k_d^2 \hat{G}^0 (\hat{U} - k_d^2 \hat{\alpha}^{\text{mm}} \hat{G}^0)^{-1} \hat{\alpha}^{\text{mm}}] \mathbf{H}, \\ \mathbf{m} &= \hat{B}^{-1} [\hat{\alpha}^{\text{mm}} + k_d^2 \hat{\alpha}^{\text{me}} \hat{G}^0 (\hat{U} - k_d^2 \hat{\alpha}^{\text{ee}} \hat{G}^0)^{-1} \hat{\alpha}^{\text{em}}] \mathbf{H}, \\ &\quad + \hat{B}^{-1} c_d \hat{\alpha}^{\text{me}} [\hat{U} + k_d^2 \hat{G}^0 (\hat{U} - k_d^2 \hat{\alpha}^{\text{ee}} \hat{G}^0)^{-1} \hat{\alpha}^{\text{ee}}] \mathbf{D}, \end{aligned} \quad (8)$$

where \hat{U} is the unit 3×3 tensor, and power -1 denotes the inverse operation applied to the corresponding matrix

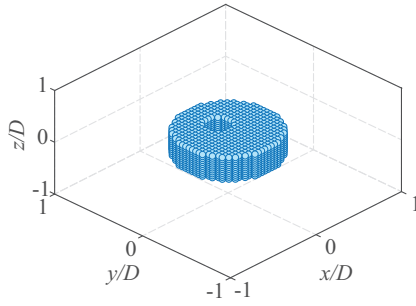


FIG. 1. Cartesian coordinate system and a dielectric nanodisk with an eccentric through hole. The hole is shifted along the y axis from the disk center. The disk is represented as a lattice of spherical elements, which are used in numerical simulations.

including \hat{A} and \hat{B} . These matrices are

$$\hat{A} = \hat{U} - k_d^2 \hat{\alpha}^{ee} \hat{G}^0 - k_d^4 \hat{\alpha}^{em} \hat{G}^0 (\hat{U} - k_d^2 \hat{\alpha}^{mm} \hat{G}^0)^{-1} \hat{\alpha}^{me} \hat{G}^0,$$

$$\hat{B} = \hat{U} - k_d^2 \hat{\alpha}^{mm} \hat{G}^0 - k_d^4 \hat{\alpha}^{me} \hat{G}^0 (\hat{U} - k_d^2 \hat{\alpha}^{ee} \hat{G}^0)^{-1} \hat{\alpha}^{em} \hat{G}^0.$$

With solution (8) the extinction cross section $\sigma_{\text{ext}}^{(1)}$ per one particle of the array can be derived in the form [7]:

$$\sigma_{\text{ext}}^{(1)} = \frac{k_d}{|\mathbf{E}|^2 \varepsilon_0 \varepsilon_d} \text{Im} \{ \mathbf{E}^* \cdot \mathbf{p} + \mu_0 \mathbf{H}^* \cdot \mathbf{m} \}, \quad (9)$$

and the transmission and reflection coefficients of the array can be calculated using the dipole approach given in Refs. [7,59,60].

The application of the above-introduced analytical approach depends on many parameters determined by the single-particle polarizabilities, array configuration, and irradiation conditions. In what follows, we apply this approach to explain mechanisms of excitation of quasi-trapped modes in a 2D array of dielectric particles with bianisotropic properties.

III. MODEL OF BIANISOTROPY AND LIGHT TRAPPING

In this section, we consider a metasurface composed of a set of identical subwavelength particles. These particles are cylindrical dielectric resonators (nanodisks, see Fig. 1). For numerical simulations, we chose the following parameters (we use approximate equality here, since the geometric parameters of the problem are determined up to the discretization step, which is 7 nm). The nanodisks' diameter and thickness are $D_c \simeq 170$ nm and $H \simeq 85$ nm, respectively. They are made of nonmagnetic material with relative permittivity $\varepsilon_p = 16$. Each nanodisk is perturbed by an eccentric through hole. The hole diameter is $D_h \simeq 50$ nm and the hole shift from the particle center along the y axis is $\Delta \simeq D_c/8$ nm. Due to the eccentric hole, the in-plane symmetry of the nanodisk is broken. The particle is symmetric with respect to the line drawn through its center parallel to the y axis, whereas with respect to the x axis it is asymmetric. Note that our results can be easily scaled for the disks with other geometrical and material parameters operating in the desired spectral range. Therefore, in what follows, we perform normalization of all geometrical parameters on the factor

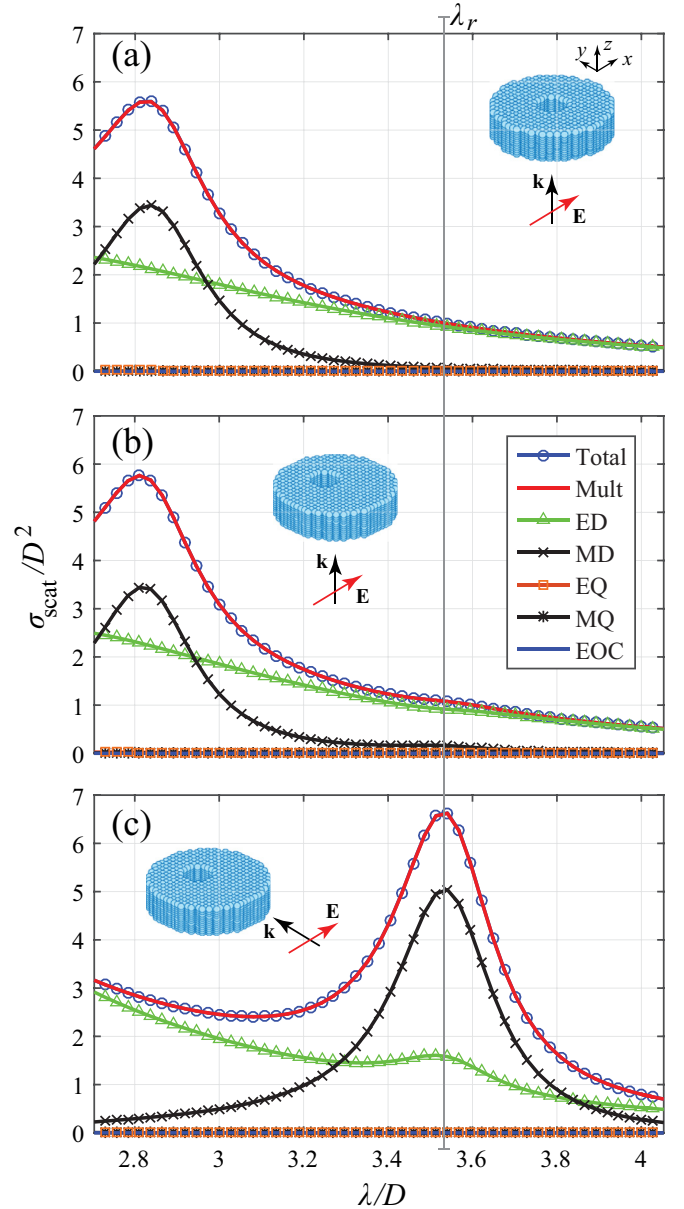


FIG. 2. Dipole and multipole contributions to the scattering cross section calculated for different irradiation conditions of the nanodisk with (a) central hole, and (b), (c) eccentric hole; in the inserts, \mathbf{k} is the wave vector and \mathbf{E} is the vector of electric field amplitude of the incident plane wave.

$D = 185$ nm. We consider for the surrounding medium $\varepsilon_d = 1$ so that $k_d = k$.

First, the optical properties of the isolated nanodisk are discussed in the context of its polarizability tensors, and the expressions describing the electric and magnetic moments of the perturbed nanodisk, with accounting for bianisotropy, are derived. For this problem, we consider a linearly polarized plane wave as exciting radiation. To derive polarizabilities, the irradiation of the nanodisk by the linearly polarized waves with different incident directions should be considered. Thus, we further distinguish x , y , and z polarizations for the incident wave. Both frontal ($\mathbf{k} = \{0, 0, \pm k_z\}$) and lateral

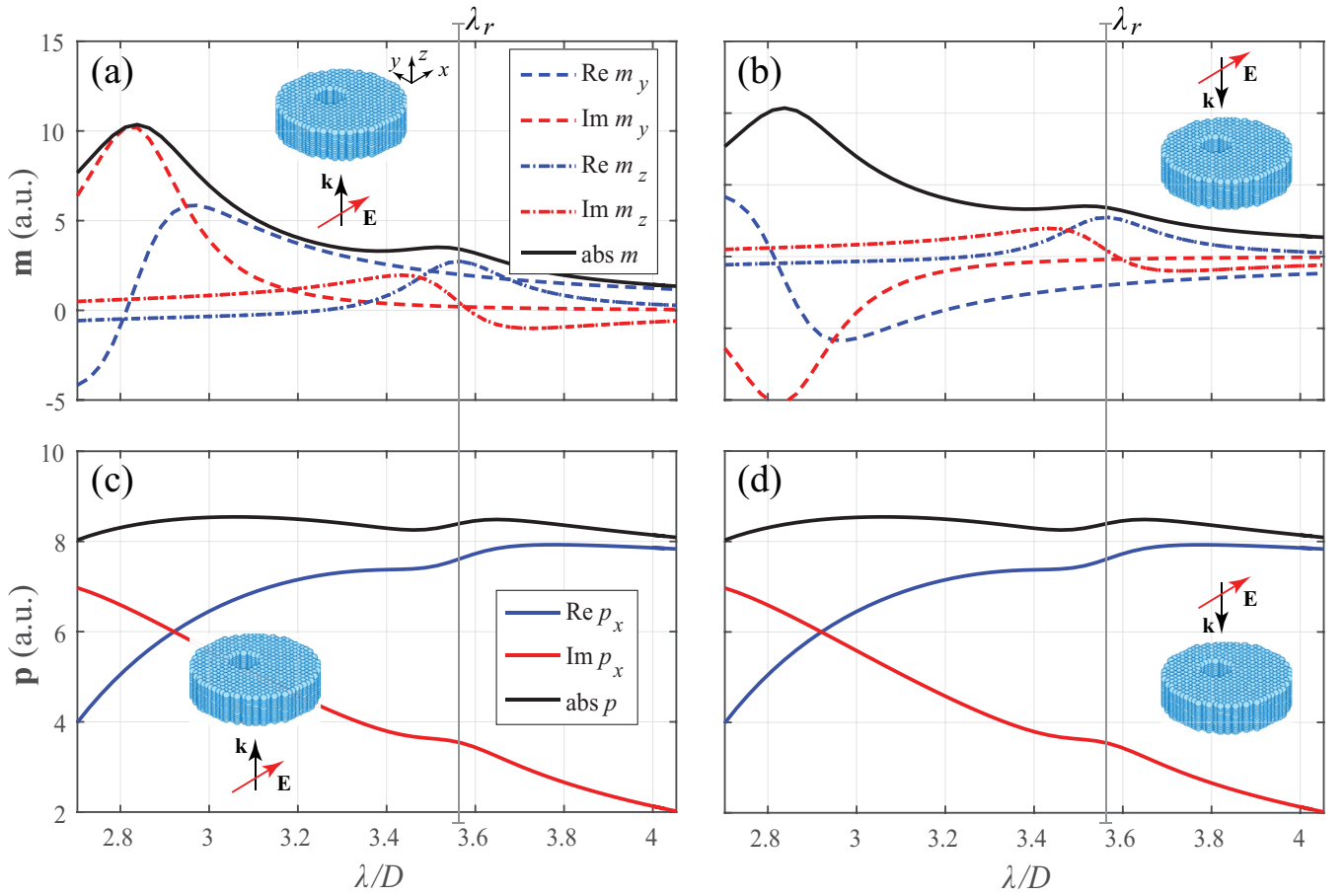


FIG. 3. Spectral characteristics of the nonzero components of (a), (b) magnetic and (c), (d) electric dipole moments and their absolute values calculated for the nanodisk irradiated by the x -polarized wave from the $+z$ and $-z$ directions as shown in the inserts. The dipoles are located at the center of nanodisk.

($\mathbf{k} = \{\pm k_x, 0, 0\} \vee \mathbf{k} = \{0, \pm k_y, 0\}$) irradiations of the nanodisk are supposed. Then we apply the obtained solution to explain characteristics of the metasurface composed of such perturbed nanodisks and irradiated by a normally incident plane wave ($\mathbf{k} = \{0, 0, +k_z\}$).

A. Bianisotropic polarizabilities of a single nanoparticle

To demonstrate the applicability of the coupled dipole approximation to the problem under study, we apply the multiple decomposition method [9] considering different irradiation conditions of the nanoparticle by the incident wave. The main multipole moments are calculated using their exact definitions from Refs. [53,54].

For numerical simulations of the disk scattering cross section we use the discrete dipole approximation (DDA) method. It allows us to obtain the distribution of the induced polarization $\mathbf{P}(\mathbf{r})$ inside an arbitrary-shaped scatterer. The main idea of the DDA method consists in the replacement of the scattering object by a cubic lattice of electric point dipoles with known polarizability. The corresponding dipole moment \mathbf{d}_j induced in each lattice point j (with the radius vector \mathbf{r}_j) is found by solving coupled dipole equations. After that a discrete representation of the induced polarization is

obtained as

$$\mathbf{P}(\mathbf{r}) = \sum_{j=1}^{N_d} \mathbf{d}_j \delta(\mathbf{r} - \mathbf{r}_j), \quad (10)$$

where N_d is the total number of the dipoles inside the scatterer, $\delta(\mathbf{r} - \mathbf{r}_j)$ is the Dirac delta function. A detailed description and discussions of the DDA numerical method and its applicability for electromagnetic scattering problems one can find in Ref. [61]. Note that there is a close correspondence between the DDA and discretizations that are based on the digitized Green's function (DGF) method or the volume-integral equation formulation (VIEF) [62].

In the framework of the DDA method, after the discretization procedure, the dielectric nanodisk is presented as a set of spherical elements (Fig. 1). Knowing the polarization \mathbf{P} , the electric field \mathbf{E}_{sca} of the wave scattered in the direction determined by a unit vector \mathbf{n} is calculated from the equation [54,63]

$$\mathbf{E}_{\text{sca}}(\mathbf{r}) = -\frac{k^2}{\varepsilon_0 4\pi r} \left[\mathbf{n} \times \left(\mathbf{n} \times \int_{V_p} e^{-ik_d(\mathbf{n}\cdot\mathbf{r}')} \mathbf{P}(\mathbf{r}') d\mathbf{r}' \right) \right], \quad (11)$$

where \mathbf{r} is the radius vector of an observation point and $\mathbf{n} = \mathbf{r}/r$, and V_p is the scatterer volume. The scattering cross section of a single scatterer is

$$\sigma_{\text{sca}} = \frac{1}{|\mathbf{E}|^2} \int_0^\pi \int_0^{2\pi} |\mathbf{E}_{\text{sca}}(\mathbf{r})|^2 r^2 d\Omega. \quad (12)$$

Multipole decomposition of the scattering cross section with accounting for the several first multipole terms is written as [54,64]

$$\begin{aligned} \sigma_{\text{sca}} \simeq & \frac{k^4}{6\pi \varepsilon_0^2 |\mathbf{E}|^2} |\mathbf{p}|^2 + \frac{k^4 \varepsilon_d \mu_0}{6\pi \varepsilon_0 |\mathbf{E}|^2} |\mathbf{m}|^2 \\ & + \frac{k^6 \varepsilon_d}{720\pi \varepsilon_0^2 |\mathbf{E}|^2} \sum_{\alpha\beta} |Q_{\alpha\beta}|^2 + \frac{k^6 \varepsilon_d^2 \mu_0}{80\pi \varepsilon_0 |\mathbf{E}|^2} \sum_{\alpha\beta} |M_{\alpha\beta}|^2 \\ & + \frac{k^8 \varepsilon_d^2}{1890\pi \varepsilon_0^2 |\mathbf{E}|^2} \sum_{\alpha\beta\gamma} |O_{\alpha\beta\gamma}|^2, \end{aligned} \quad (13)$$

where \mathbf{p} and \mathbf{m} are the vectors of electric and magnetic dipole moments of the scatterer, respectively, and \hat{Q} , \hat{M} , and \hat{O} are the tensors of electric and magnetic quadrupole moments, and electric octupole moment, respectively. Definitions of the multipole moments can be found elsewhere [53,54], whereas expressions for the electric and magnetic dipole moments are given below.

The resulting contributions of the corresponding dipolar and multipolar moments to the scattering cross section of the given nanoparticle are shown in Fig. 2. From this figure, one can conclude that only electric dipole (ED) and magnetic dipole (MD) make a major contribution to the total scattering cross section independently on the irradiation conditions. Contributions of the higher-order multipoles, such as electric quadrupole (EQ), magnetic quadrupole (MQ), electric octupole (EOC), and others, are negligibly small. It means that the optical response of the chosen nanodisk can be adequately described in the dipole approximation.

Comparing the curves presented in Figs. 2(a) and 2(b) one can see that as soon as a perturbation to the nanodisk is introduced (i.e., the hole is shifted from the nanodisk's center) an additional weak dipole resonance appears at the wavelength $\lambda_r \approx 660$ nm ($\lambda_r/D \approx 3.57$). This resonance is attributed to the trapped mode, which is a signature of the systems with broken symmetry [20]. Importantly, the spectral position of this additional resonance coincides with both frontal and lateral irradiation of the nanoparticle. Below we show that this additional resonance is a manifestation of the effect of bianisotropy induced by the in-plane broken symmetry.

Dipole polarizability tensor of a single nanoparticle can be calculated using the approach given in Refs. [41,42]. Initially, one has to calculate the electric and magnetic dipole moments induced separately by mutually inverse incident plane waves with the same linear electric polarization. For example, if we consider the incident x -polarized waves propagating in the $+z$ and $-z$ directions (see the inserts in Fig. 3) electric \mathbf{p} and magnetic \mathbf{m} dipole moments should satisfy the following expressions:

$$\begin{aligned} p_j^\pm &= \alpha_{jx}^{\text{ee}} D_0 \pm \alpha_{jy}^{\text{em}} D_0, \\ c_d^{-1} m_j^\pm &= \pm \alpha_{jy}^{\text{mm}} D_0 + \alpha_{jx}^{\text{me}} D_0, \end{aligned} \quad (14)$$

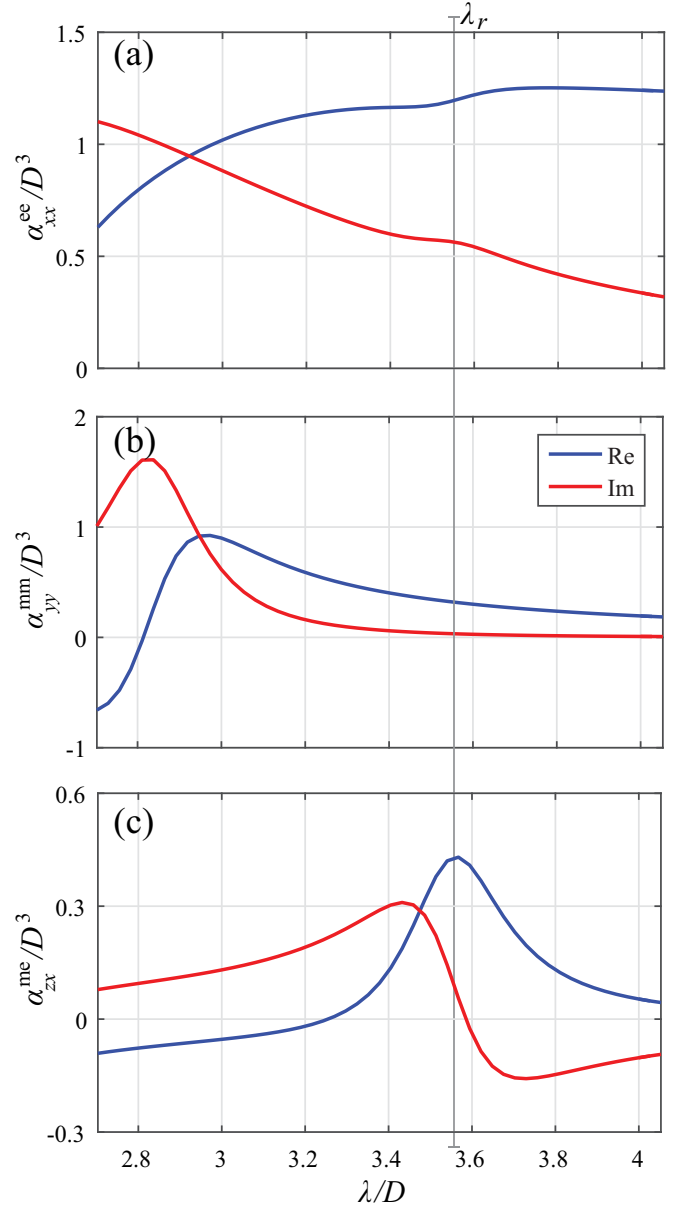


FIG. 4. Spectral characteristics of the nonzero components of the dipole (a) electric, (b) magnetic, and (c) magnetoelectric polarizabilities calculated for the problem geometries presented in Fig. 3.

where the sign choice corresponds to the incident wave propagation direction, $j = x, y, z$, the dipole moments are located at the origin of the coordinate system (see Fig. 1), and

$$\begin{aligned} \mathbf{D} &= \{D_0, 0, 0\} e^{\pm ikz}, \\ \mathbf{H} &= \{0, \pm c_d D_0, 0\} e^{\pm ikz}, \end{aligned} \quad (15)$$

where $D_0 = \varepsilon_0 \varepsilon_d E$ is the amplitude of \mathbf{D} .

Solving system (14) yields the polarizability components

$$\begin{aligned} \alpha_{jx}^{\text{ee}} &= \frac{p_j^+ + p_j^-}{2D_0}, & \alpha_{jy}^{\text{em}} &= \frac{p_j^+ - p_j^-}{2D_0}, \\ \alpha_{jy}^{\text{mm}} &= \frac{m_j^+ - m_j^-}{2c_d D_0}, & \alpha_{jx}^{\text{me}} &= \frac{m_j^+ + m_j^-}{2c_d D_0}, \end{aligned} \quad (16)$$

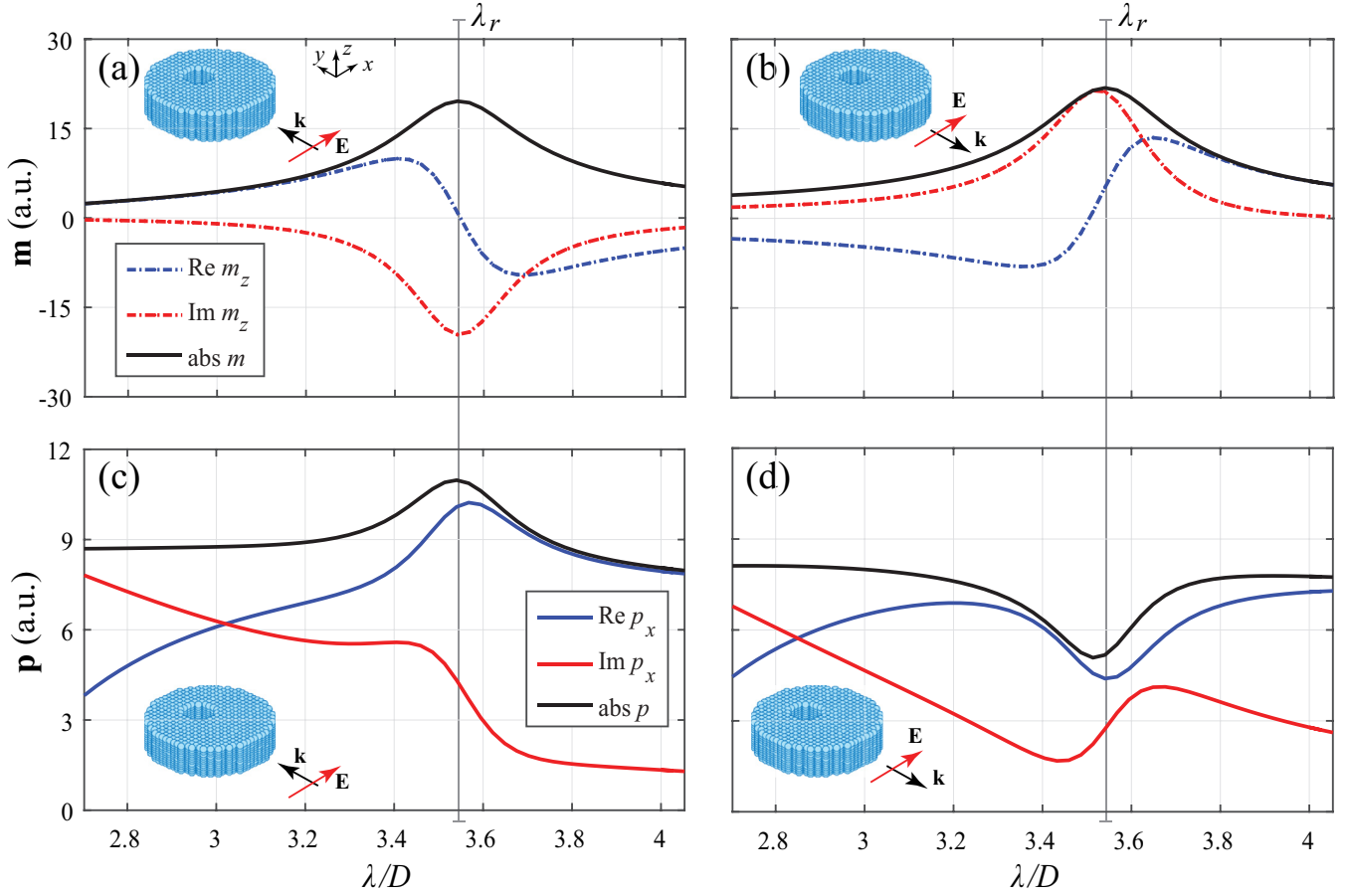


FIG. 5. The same as in Fig. 3 but for the lateral irradiation of the nanodisk from the $+y$ and $-y$ directions; (a), (b) magnetic and (c), (d) electric dipole moments.

where the electric and magnetic dipole moments are related to the total electric field induced inside the particle [53,54]. They are

$$\begin{aligned} \mathbf{p}^\pm &= \int_{V_p} j_0(k_d r) \mathbf{P}^\pm(\mathbf{r}) d\mathbf{r} \\ &+ \frac{k_d^2}{2} \int_{V_p} \frac{j_2(k_d r)}{(k_d r)^2} [3(\mathbf{r} \cdot \mathbf{P}^\pm(\mathbf{r}))\mathbf{r} - r^2 \mathbf{P}^\pm(\mathbf{r})] d\mathbf{r}, \\ \mathbf{m}^\pm &= \frac{\omega}{2i} \int_{V_p} \frac{j_1(k_d r)}{k_d r} [\mathbf{r} \times \mathbf{P}^\pm(\mathbf{r})] d\mathbf{r}, \end{aligned} \quad (17)$$

where V_p is the scatterer volume, $j_0(k_d r)$, $j_1(k_d r)$, and $j_2(k_d r)$ are the zero-, first-, and second-order spherical Bessel functions [53,54], and $\mathbf{P}^\pm(\mathbf{r}) = (i/\omega)\mathbf{j}^\pm(\mathbf{r})$ is the induced polarization $\mathbf{P}^\pm(\mathbf{r})$ or electric current density $\mathbf{j}^\pm(\mathbf{r})$ inside the particle. Note that inside the scatterer, the induced polarization is related to the total electric field as $\mathbf{P}^\pm(\mathbf{r}) = \varepsilon_0(\varepsilon_p - \varepsilon_d)\mathbf{E}^\pm(\mathbf{r})$.

Results of the dipole moments calculation for the frontal irradiation of the nanodisk by the x -polarized wave from the $+z$ and $-z$ directions are summarized in Fig. 3. One can see that the magnetic dipole vector has two nonzero components m_y and m_z [see Figs. 3(a) and 3(b)]. Remarkably, the sign of m_z does not depend on the direction of incidence of the irradiating wave, whereas m_y changes the sign correspond-

ingly. This is because the characteristic of the m_z component is determined by the direction of the incident electric field, while that of the m_y component depends on the direction of the incident magnetic field, which is an axial vector dependent on the geometry of the given problem. This dependence on the sign of the components of the magnetic dipole vector on the direction of the incident wave irradiation expresses the essence of bianisotropy in the asymmetric nanoparticle. Also from Figs. 3(c) and 3(d) one can conclude that the electric dipole vector has only one component p_x which is independent on the incident wave irradiation direction. It means that p_x is solely determined by the characteristics of the electric field. Applying Eq. (16) for the numerically calculated values presented in Fig. 3, the nonzero components of the dipole polarizability tensors α_{yy}^{mm} , α_{zx}^{me} , and α_{xx}^{ee} can be obtained. The results of the corresponding calculations are presented in Fig. 4.

The electromagnetic response of the nanodisk on the lateral irradiation can be revealed similarly to the above-presented frontal case. Figure 5 demonstrates the magnetic \mathbf{m} and electric \mathbf{p} dipole moments calculated for the lateral irradiation of the nanodisk from the $+y$ and $-y$ directions. It is evident that for this problem geometry there is a strong dependence of the induced magnetic and electric dipoles on the irradiation direction of the incident wave. The corresponding

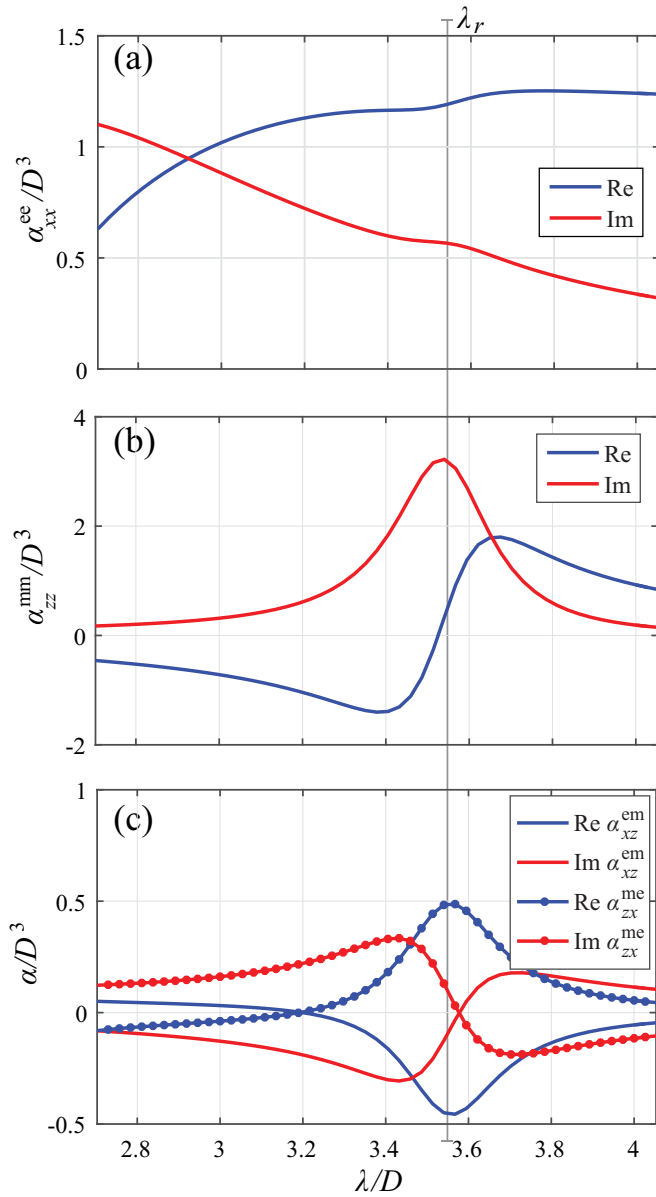


FIG. 6. Spectral characteristics of the nonzero components of the dipole (a) electric, (b) magnetic, and (c) electromagnetic and magnetoelectric polarizabilities calculated for the problem geometries presented in Fig. 5.

nonzero polarizabilities are collected in Fig. 6. The effect of bianisotropy manifests itself in the resonant behaviors of the cross polarizabilities α_{xz}^{me} and α_{zx}^{em} [Fig. 6(c)]. One can see that for these cross polarizabilities the condition $\alpha_{zx}^{me} \approx -\alpha_{xz}^{em}$ holds, which complies with the Onsager-Casimir principle [65] (some mismatch in the coincidence of the curves can be explained by the finiteness of discretization in the numerical simulation). An account for other cases when the nanodisk is irradiated by the z -polarized wave incident from the $\pm x$ and $\pm y$ directions gives us the rest components of the polarizability tensors. Here $\alpha_{xx}^{mm} \approx \alpha_{yy}^{mm}$, while other nonzero polarizability components are not presented here, since they are inessential for our subsequent consideration.

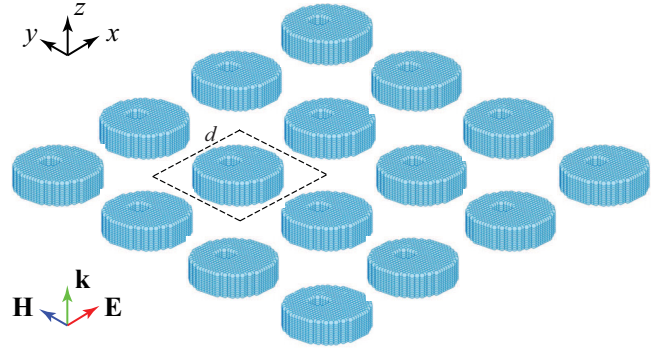


FIG. 7. Schematic view of an all-dielectric metasurface composed of perturbed nanodisks and the irradiation condition.

A principal conclusion to this section is that the strong resonant bianisotropic response appears in the in-plane perturbed dielectric nanodisks. It is related to the excitation of the out-of-plane (directed along the z axis) component m_z of the magnetic dipole moment. The spectral position of this resonance coincides with that of the magnetic dipole resonance excited under the lateral irradiation conditions. Such a resonant feature allows us to realize an excitation of the trapped mode in a 2D array composed of such perturbed nanodisks.

B. Trapping light in a 2D array of nanodisks

In this section, we show that due to the bianisotropic properties of the perturbed nanodisk, a 2D periodic array composed of such nanodisks can support an ultranarrow optical resonance in the reflection and transmission spectra. This resonance is related to the trapped mode and corresponds to the electromagnetic coupling of the out-of-plane components of magnetic dipole moments induced in the nanodisks by an external electromagnetic wave.

We consider a metasurface that is infinitely distributed in the x - y plane at $z = 0$ embedded in a homogeneous nonmagnetic transparent medium with a relative dielectric constant $\varepsilon_d = 1$. Perturbed nanodisks are oriented equally and arranged equidistantly forming a metasurface array. The array has a lattice period d in both the x and y directions (Fig. 7). The metasurface is irradiated by the x -polarized plane wave propagating in the $+z$ direction with the magnetic field vector oriented along the y axis (Fig. 7). In the chosen problem geometry, the electromagnetic field of the incident wave excites only one component p_x of the electric dipole moment and two components m_y and m_z of the magnetic dipole moment in each nanodisk forming the array. Therefore, from Eq. (6) we can write

$$\begin{aligned} p_x &= \alpha_{xx}^{ee} [D_x + k_d^2 G_{xx}^0 p_x] + c_d^{-1} \alpha_{xz}^{em} k_d^2 G_{zz}^0 m_z, \\ m_z &= \alpha_{zz}^{mm} k_d^2 G_{zz}^0 m_z + c_d \alpha_{zx}^{me} [D_x + k_d^2 G_{xx}^0 p_x], \\ m_y &= \alpha_{yy}^{mm} [H_y + k_d^2 G_{yy}^0 m_y]. \end{aligned} \quad (18)$$

Here only corresponding nonzero components of the polarizability tensors are taken into account, and, due to the structure periodicity in the x and y directions, the tensor \hat{G}^0 , composed of the dipole sums, contains only the nonzero diagonal ele-

ments G_{xx}^0 , G_{yy}^0 , and G_{zz}^0 [58,66]. For the periodic array with square unit cell, the condition $G_{xx}^0 = G_{yy}^0$ holds. The remaining elements are

$$\hat{G}_{xx}^0 = \frac{1}{4\pi} \sum_{l=2}^{\infty} \frac{e^{ik_d r_l}}{r_l} \left(1 + \frac{i}{k_d r_l} - \frac{1}{k_d^2 r_l^2} - \frac{x_l^2}{r_l^2} - \frac{i3x_l^2}{k_d r_l^3} + \frac{3x_l^2}{k_d^2 r_l^4} \right), \quad (19)$$

$$\hat{G}_{zz}^0 = \frac{1}{4\pi} \sum_{l=2}^{\infty} \frac{e^{ik_d r_l}}{r_l} \left(1 + \frac{i}{k_d r_l} - \frac{1}{k_d^2 r_l^2} \right), \quad (20)$$

where $r_l = \sqrt{x_l^2 + y_l^2}$ is the distance between the Cartesian coordinate system origin, which coincides with position of the magnetic and electric dipoles of the nanodisk with number $l = 1$, and other points where the dipoles of nanodisks with number $l \geq 2$ are located. Note that the expressions for the dipole sums G_{yy}^0 and G_{zz}^0 can be obtained from Eq. (19) by simple replacing x_l with y_l and z_l , respectively. In the latter case for getting Eq. (20), one has to put $z_l = 0$ because all dipoles are located in the x - y plane with $z = 0$.

1. Trapped mode

Before proceeding with the analysis of Eq. (18), let us consider a hypothetical case. Assume that all particles in the infinite array of disks possess only z component of the magnetic dipole moment m_z without any external field sources. Also in the array, there is not any coupling to components of all other existing magnetic and electric dipoles. In this case system (18) can be reduced to the equation

$$(1 - \alpha_{zz}^{\text{mm}} k_d^2 G_{zz}^0) m_z = 0. \quad (21)$$

For Eq. (21) to have a nontrivial solution ($m_z \neq 0$), the following condition must be satisfied:

$$\alpha_{zz}^{\text{mm}} k_d^2 G_{zz}^0 = 1. \quad (22)$$

Now we show that this condition can be fully satisfied only for the case of lossless dipole particles.

Introducing new notations $\alpha_{zz}^{\text{mm}} = \alpha'_z + i\alpha''_z$ and $k_d^2 G_{zz}^0 = S'_z + iS''_z$, where α'_z and S'_z are the real parts and α''_z and S''_z are the imaginary parts of the corresponding values, Eq. (22) has the following solution:

$$\begin{aligned} S'_z &= \frac{\alpha'_z}{\alpha_z'^2 + \alpha_z''^2} \equiv \text{Re} \frac{1}{\alpha_{zz}^{\text{mm}}}, \\ S''_z &= -\frac{\alpha_z''}{\alpha_z'^2 + \alpha_z''^2} \equiv \text{Im} \frac{1}{\alpha_{zz}^{\text{mm}}}. \end{aligned} \quad (23)$$

It expresses the conditions of the m_z -lattice mode existence, which can be referred to as a trapped mode. Such a reference is valid since for this mode there is no electromagnetic energy radiation from the array plane to free space due to z orientation of all magnetic dipoles. With this solution we can analyze the feasibility of the trapped mode in a realistic structure.

If $d < 2\pi/k_d$, then the summation in S''_z can be performed analytically, resulting in

$$\begin{aligned} S''_z &\equiv \frac{k_d^2}{4\pi} \sum_{l,j=0,1,2,\dots}^{\infty} \left(\frac{\sin k_d d_{lj}}{d_{lj}} + \frac{\cos k_d d_{lj}}{k_d d_{lj}^2} - \frac{\sin k_d d_{lj}}{k_d^2 d_{lj}^3} \right) \\ &= -\frac{k_d^3}{6\pi}, \end{aligned} \quad (24)$$

where $d_{lj} = d\sqrt{l^2 + j^2}$, $k_d = 2\pi/\lambda_d$ is the wave number, $\lambda_d = \lambda/\sqrt{\epsilon_d}$ is the wavelength in the surrounding lossless medium, and the term with $d_{00} = 0$ is excluded from the sum. From the obtained expression one can notice that S''_z is dependent on the wavelength λ_d and independent on the period d .

For the real part of S_z we have

$$S'_z = \frac{k_d^2}{4\pi} \sum_{l,j=0,1,2,\dots}^{\infty} \left(\frac{\cos k_d d_{lj}}{d_{lj}} - \frac{\sin k_d d_{lj}}{k_d d_{lj}^2} - \frac{\cos k_d d_{lj}}{k_d^2 d_{lj}^3} \right). \quad (25)$$

Here again the term with $d_{00} = 0$ is excluded from the sum. In contrast to the characteristic of S''_z , the sum S'_z is slowly converged, therefore it has to be evaluated numerically. Remarkably, S'_z is dependent on both the wavelength λ_d and period d .

From the ratio between the extinction cross section, which is calculated involving the optical theorem, and the scattering cross section for a dipole lossless scatterer [64], one can obtain the general equality for the imaginary part of $1/\alpha_{zz}^{\text{mm}}$

$$\text{Im} \frac{1}{\alpha'_z + i\alpha''_z} = -\frac{\alpha''_z}{\alpha_z'^2 + \alpha_z''^2} = -\frac{k_d^3}{6\pi}, \quad (26)$$

which is completely independent on the scatterer design [67]. Comparing Eqs. (24) and (26) one can see that the second condition for S''_z in Eq. (23) is always satisfied for a dipole lossless scatterer. Thus the condition of the trapped mode existence is determined by the first equation in system (23).

Figure 8(a) demonstrates the spectral dependence of the value S'_z calculated for different d . One can see that the value S'_z changes its sign from positive to negative as the wavelength increases. The larger array period, the larger wavelength λ_0 at which the value S'_z crosses zero. The spectral characteristics of $\text{Re}(1/\alpha_{zz}^{\text{mm}})$ and $\text{Im}(1/\alpha_{zz}^{\text{mm}})$ are presented in Figs. 8(a) and 8(b), respectively. The inverse polarizability is calculated in correspondence to parameters given in Fig. 6(b) for the disk with bianisotropic properties. Comparing the curves for S'_z and $\text{Re}(1/\alpha_{zz}^{\text{mm}})$ presented in Fig. 8(a), one can see that the condition $S'_z = \text{Re}(1/\alpha_{zz}^{\text{mm}})$ holds for the trapped mode for all shown periods. It is always possible to tune the realization of this condition on a specified wavelength by varying the array period, since the value S'_z is independent on the nanoparticle polarizability. Contrariwise, as Fig. 8(b) suggests regarding imaginary part of S_z , the inequality $\text{Im}(1/\alpha_{zz}^{\text{mm}}) < -k_d^3/6\pi \equiv S''_z$ appears, which means that there is an energy leakage for the trapped mode (i.e., it turns to a weakly radiating state). This inequality follows from the energy conservation law and magnetoelectric optical theorem [68,69] introduced for the dynamic polarizability tensor accounting for the bianisotropic terms in the lossless case. In the given problem, due to

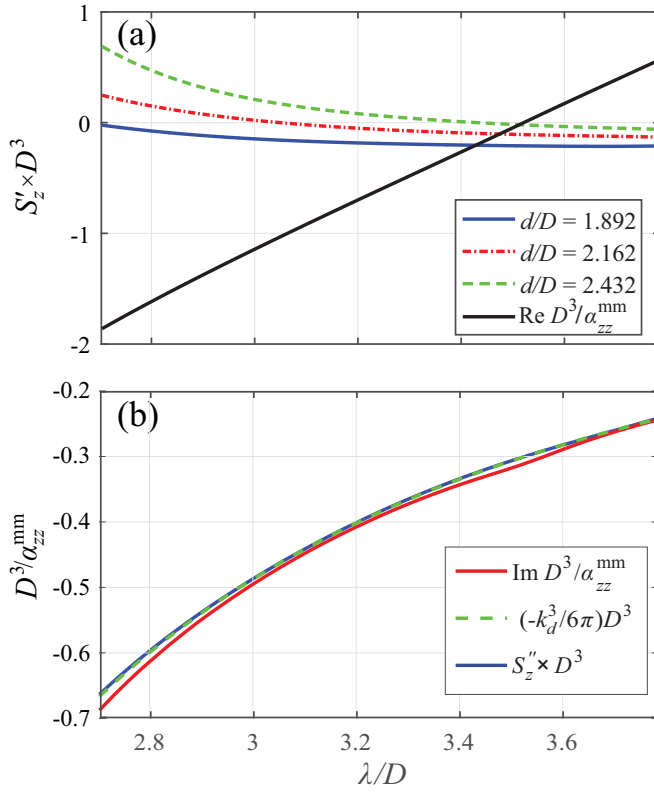


FIG. 8. (a) Spectral dependence of the value S'_z calculated numerically according to Eq. (25) for several values of the period d , and spectral dependence of the real part of the inverse polarizability $1/\alpha_{zz}^{\text{mm}}$. The metasurface under study is disposed in air ($\epsilon_d = 1$). (b) Imaginary part of the inverse polarizability $1/\alpha_{zz}^{\text{mm}}$ and the imaginary part S'_z calculated numerically from the sum in Eq. (24) and compared with $-k_d^3/6\pi$.

bianisotropy, condition (26) is reduced to

$$\text{Im} \frac{1}{\alpha_{zz}^{\text{mm}}} = -\frac{k_d^3}{6\pi} \left(1 + \frac{|\alpha_{xz}^{\text{em}}|^2}{|\alpha_{zz}^{\text{mm}}|^2} \right). \quad (27)$$

Therefore, the introducing bianisotropy into particles opens a channel for the trapped mode excitation by electromagnetic plane waves normally incident on the array. However, the channel opening also leads to the energy leakage transforming nonradiating trapped mode to the radiating one. The energy leakage is characterized by the second term in the brackets of Eq. (27). In what follows we refer to this weakly radiating state as a quasi-trapped mode.

2. Quasi-trapped mode

The solution of system (18) can be written as

$$p_x = K^{-1} [\alpha_{xx}^{\text{ee}} (1 - \alpha_{zz}^{\text{mm}} k_d^2 G_{zz}^0) + \alpha_{xz}^{\text{em}} k_d^2 G_{zz}^0 \alpha_{zx}^{\text{me}}] D_x \equiv \alpha_{xx}^{\text{ee/eff}} D_x, \quad (28)$$

$$m_z = K^{-1} \alpha_{zx}^{\text{me}} c_d D_x \equiv \alpha_{zx}^{\text{me/eff}} c_d D_x, \quad (29)$$

and

$$m_y = \frac{1}{1/\alpha_{yy}^{\text{mm}} - k_d^2 G_{yy}^0} H_y \equiv \alpha_{yy}^{\text{mm/eff}} H_y, \quad (30)$$

where

$$K = (1 - \alpha_{xx}^{\text{ee}} k_d^2 G_{xx}^0) (1 - \alpha_{zz}^{\text{mm}} k_d^2 G_{zz}^0) - \alpha_{xz}^{\text{em}} k_d^2 G_{zz}^0 \alpha_{zx}^{\text{me}} k_d^2 G_{xx}^0, \quad (31)$$

and the corresponding effective polarizabilities $\alpha_{xx}^{\text{ee/eff}}$, $\alpha_{zx}^{\text{me/eff}}$, and $\alpha_{yy}^{\text{mm/eff}}$ are introduced. Identical denominator K of expressions (28) and (29) indicates on strong coupling and same resonant behavior of p_x and m_z . For p_x the next expression can be formally written

$$p_x = p_x^0 + p_x^m, \quad (32)$$

where

$$p_x^0 = K^{-1} \alpha_{xx}^{\text{ee}} (1 - \alpha_{zz}^{\text{mm}} k_d^2 G_{zz}^0) D_x \quad (33)$$

is the part of p_x , which is mainly excited by the field of incident wave, and

$$p_x^m = c_d^{-1} \alpha_{xz}^{\text{em}} k_d^2 G_{zz}^0 m_z \quad (34)$$

is the part excited due to the bianisotropic coupling with the field generated by m_z .

Expression (9) for the extinction cross section produced by a single particle in the array can be written as

$$\sigma_{\text{ext}}^{(1)} = \frac{k_d \epsilon_0 \epsilon_d}{|D_x|^2} \text{Im} \{ E_x^* p_x + \mu_0 H_y^* m_y \}. \quad (35)$$

Taking into account Eq. (32) it is seen that $\sigma_{\text{ext}}^{(1)}$ is also depended on the out-of-plane magnetic dipole component m_z . Finally, we have

$$\sigma_{\text{ext}}^{(1)} = k_d \text{Im} \{ \alpha_{xx}^{\text{ee/eff}} + \alpha_{yy}^{\text{mm/eff}} \}. \quad (36)$$

Similarly to the extinction cross sections given by Eq. (9), the reflection r and transmission t coefficients of the metasurface can be formally determined via the in-plane dipole components p_x and m_y , since only these components radiate in the perpendicular directions with respect to the metasurface plane. These coefficients are [7,59,60]

$$r = \frac{ik_d}{2D_x S_L} \left[p_x - \frac{1}{c_d} m_y \right], \quad (37)$$

$$t = 1 + \frac{ik_d}{2D_x S_L} \left[p_x + \frac{1}{c_d} m_y \right], \quad (38)$$

where S_L is the area of the array unit cell, and the contribution of the out-of-plane component m_z enters owing to the bianisotropic coupling with p_x [see Eq. (32)]. The intensity reflection R and transmission T coefficients are

$$R = |r|^2, \quad T = |t|^2, \quad (39)$$

and the absorption coefficient A can be obtained from the electromagnetic energy conservation relation $A = 1 - T - R$.

We apply the developed model to analyze the optical properties of the metasurface presented in Fig. 7 substituting nanodisks by their electric and magnetic dipoles. For the

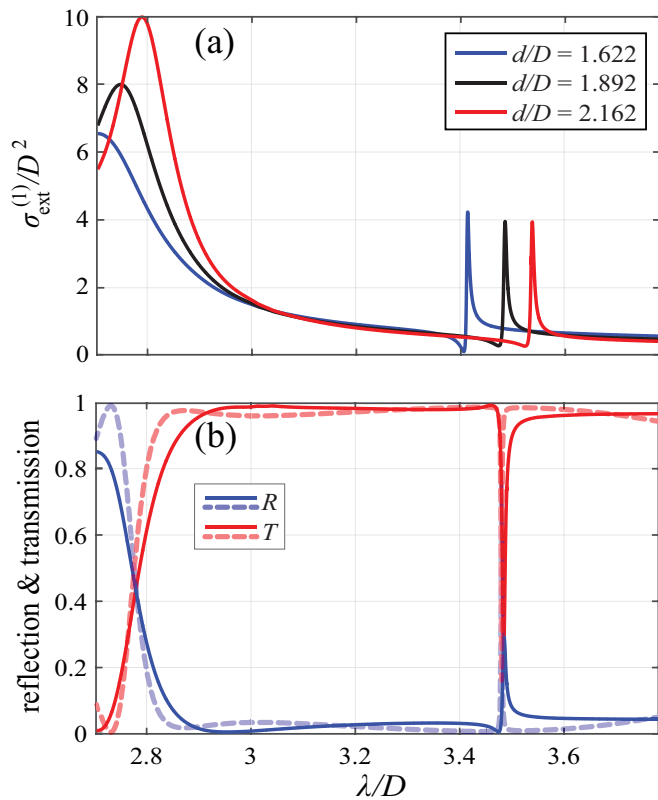


FIG. 9. (a) Extinction cross section per one particle for several values of the period p of the all-dielectric metasurface, and (b) reflection and transmission spectra of the metasurface composed of array with the lattice period $d/D = 1.892$ calculated with the coupled dipole approximation (solid lines) and full-wave simulation (dashed lines).

numerical evaluations of the dipole sums G_{xx}^0 and G_{yy}^0 we use useful analytical relation from Ref. [70]:

$$k_d \text{Im} G_{xx}^0 = k_d \text{Im} G_{yy}^0 = \frac{k_d}{2S_L} - \frac{k_d^3}{6\pi}, \quad d < 2\pi/k_d, \quad (40)$$

and for G_{zz}^0 we use Eq. (24).

The spectral dependences of the extinction cross sections per one particle for the metasurfaces with different period d are shown in Fig. 9(a). Also the reflection and transmission spectra of the metasurface calculated with the developed coupled dipole approximation are presented in Fig. 9(b) by solid lines. These results are checked against full-wave simulations by the RF Module of the COMSOL MULTIPHYSICS solver. Since the parameters of the developed model have a certain degree of inaccuracy associated with the discretization step, the following parameters are specified for full-wave simulations: $D_c = 170$ nm, $H = 85$ nm, $D_h = 40$ nm, $\Delta = D_c/8$, and $d = 350$ nm. The results of full-wave simulations are shown in Fig. 9(b) by dashed lines and agree closely with our analytical findings. This clearly verifies the obtained solution.

Figure 9 suggests that there are two types of resonances in the chosen wavelength range: a shortwave broad resonance and longwave narrow resonance with high quality factor. The longwave resonance acquires a peak-and-trough (Fano) profile [38] (for the definition of the quality factor of a Fano

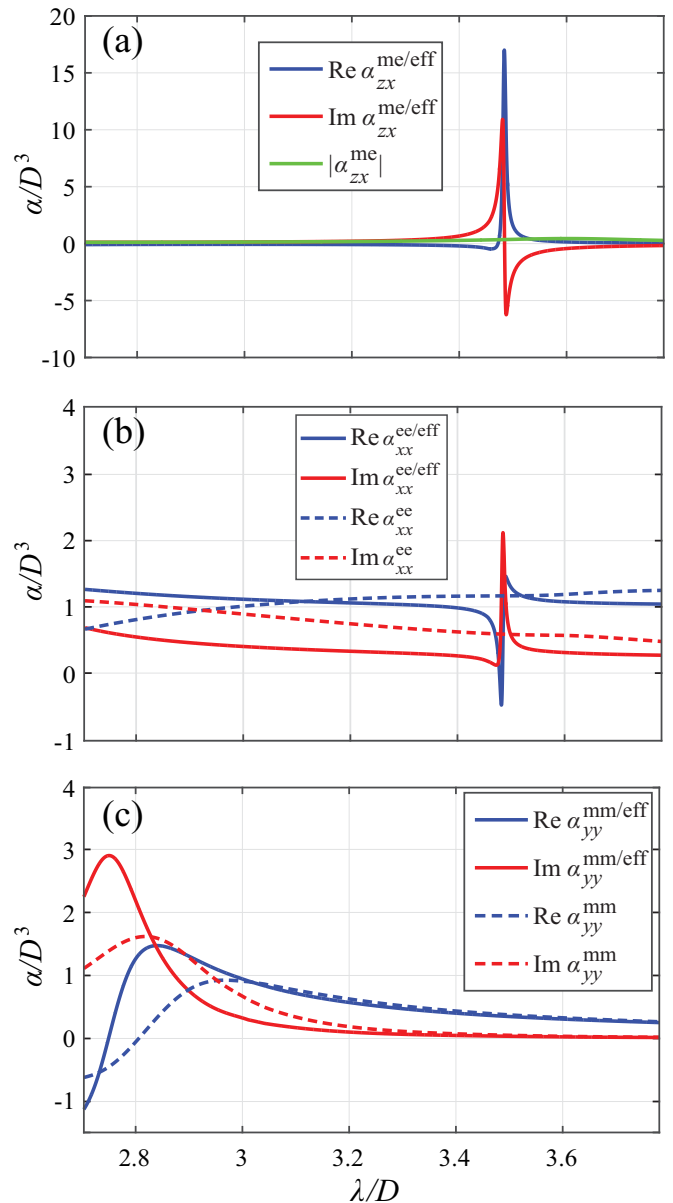


FIG. 10. Comparative characteristics of polarizabilities of the singly standing perturbed nanodisk and the same perturbed nanodisks disposed in the array with period $d/D = 1.892$. They are related to (a) m_z , (b) p_x , and (c) m_y dipole components.

resonance, see Refs. [71,72]). Increasing the lattice period induces a wavelength to downshift for both resonances which indicate existing lattice coupling between nanodisks in the array.

The corresponding narrow longwave resonance in the reflection and transmission spectra appears as a result of the bianisotropic coupling between the p_x and m_z dipole components. This conclusion is made after comparing the curves in Figs. 9 and 10. Thus, in Fig. 10 the spectral characteristics of polarizabilities of the singly standing perturbed nanodisk and the effective polarizabilities of the same perturbed nanodisks arranged in the metasurface are given. The extreme quality factor growth of the p_x and m_z resonances is related to the quasi-trapped mode excitation for which the strong

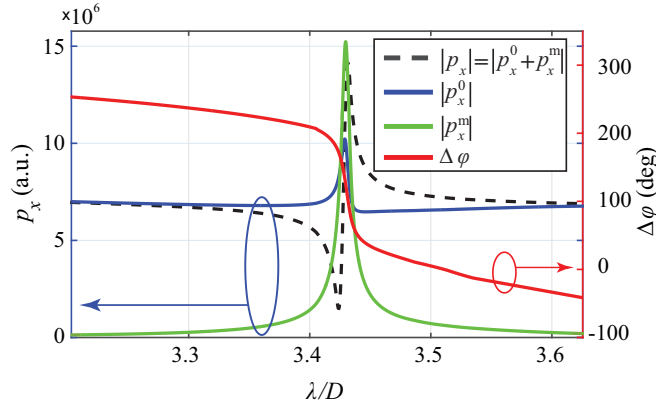


FIG. 11. Spectral behaviors of $|p_x|$ and contributions p_x^0 and p_x^m , and the phase difference $\Delta\varphi$ between these contributions.

suppression of radiation losses is evident for the m_z component. We emphasize that this effect is related to bianisotropy of the second type discussed in Ref. [51] and corresponding to the omega meta-atom effect. Note that, for the trapped mode, the bianisotropic part of the magnetic moment m_z is induced by the orthogonal electric field E_x .

The Fano profile of the long-wave resonances depicted in Fig. 9 results from the interference coupling between two contributions in the excitation of p_x . In Eq. (32), the first term p_x^0 is associated with the broadband excitation directly from free space, and the second term p_x^m corresponds to the narrow-band excitation from the trapped mode. From Fig. 11 one can conclude that on the shortwave side of the p_x resonance, the contributions from free space (p_x^0) and from the trapped mode (p_x^m) are out-of-phase ($\Delta\varphi \simeq 180^\circ$) resulting in the suppression of p_x . This suppression explains the local dips of the extinction spectra presented in Fig. 9(a).

Thus, the physical mechanism providing ultranarrow resonances in the reflection and transmission spectra of the given metasurface can be explained as follows: (i) Due to the bianisotropic property of the perturbed nanoparticles forming the metasurface, normally incident electromagnetic waves excite the out-of-plane (m_z) component of the magnetic dipole moment in each nanoparticle. The magnetic moments of all particles are oriented identically. (ii) These out-of-plane magnetic moments do not radiate electromagnetic waves from the metasurface plane, but can resonantly radiate in the longitudinal directions along the metasurface plane. (iii) When the conditions for the trapped mode excitation are satisfied, the resonant coupling between the out-of-plane magnetic dipole components m_z significantly suppresses their radiation in the longitudinal directions, which increases the quality factor of the out-of-plane dipole resonance. (iv) However, the effect of bianisotropy opens not only the channel for the excitation of the trapped mode but also enables the energy leakage, which complies with the reciprocity theorem [73]. There is a bianisotropic coupling between the out-of-plane and in-plane dipole components that radiate the electromagnetic energy from the array plane into the far-field zone. In these conditions, the excited mode can be considered as a quasi-trapped mode resulting in the arising narrow resonance in the metasurface reflection and transmission spectra. Nevertheless,

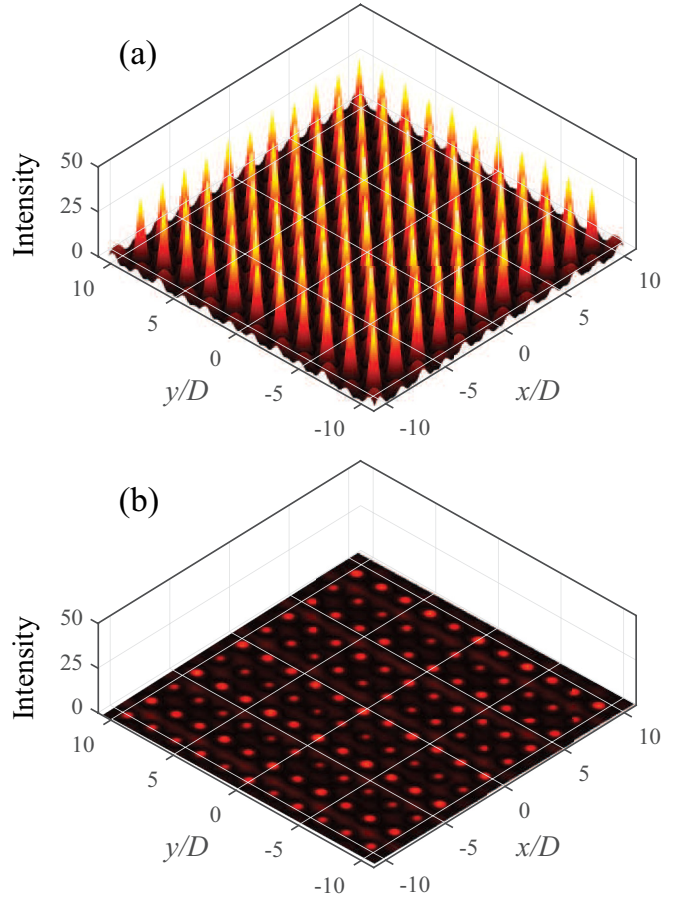


FIG. 12. Normalized intensity of the z component of magnetic field mapped in the x - y plane at position $z/D = 0.8108$ above the metasurface at the wavelength of (a) the resonant quasi-trapped mode excitation and (b) far from the resonance. The plotted intensities are normalized on the incident wave intensity.

despite a small leakage of energy, the electromagnetic field is still strongly confined in the metasurface plane at the resonant wavelength (see Fig. 12).

Note, that the resonant coupling of the m_z component between the particles in the array may also exist without bianisotropy due to resonant behaviors of the magnetic dipole polarizability α_{zz}^{mm} . It means that the role of bianisotropy is only in the opening a channel for the trapped mode excitation. If one finds a way to close this channel after the mode is excited, the electromagnetic energy will be stored in the trapped mode without any leakage.

IV. CONCLUSION

The coupled dipole equation method has been applied to study the optical response of an infinite metasurface composed of dielectric disks with bianisotropic properties. First, the generalized equations for describing electric and magnetic dipole vectors via dyadic polarizabilities were obtained. Next, the electric and magnetic moments of an isolated nanodisk perturbed by an eccentric through hole were calculated and analyzed, with accounting for bianisotropy. Finally, the obtained solution was applied to study resonant conditions of

the trapped mode excitation in an all-dielectric metasurface composed of such perturbed nanodisks and irradiated by a normally incident electromagnetic wave. For this metasurface, we reported on the observation of exceptionally narrow transmission and reflection resonances, which are attributed to the excitation of the trapped mode through the free-space coupling, which is provided by the structural symmetry breaking.

We concluded that the trapped mode of an all-dielectric metasurface is realized due to the lattice coupling between out-of-plane multipole moments of individual disks forming the metasurface when these moments do not radiate collectively electromagnetic waves from the metasurface plane. In this meaning, the trapped modes are identical to the symmetry-protected bound states in the continuum supported by the periodic nanoparticle arrays.

The obtained solution allows us to gain a deeper understanding of the mechanism of excitation of the trapped modes in all-dielectric metasurfaces and to determine the impact of bianisotropy of individual resonators on the electromagnetic features of the entire nanostructure. This opens prospects in

the conscious design of tiny optical devices by using novel resonant low-loss all-dielectric metasurfaces with active and nonlinear media inclusions. These artificial open high-quality-factor two-dimensional periodic nanostructures are promising to achieve strong localization and enhancement of electromagnetic fields, which is necessary to produce effectively tunable metasurfaces.

ACKNOWLEDGMENTS

A.B.E. and B.N.C. acknowledge financial support from the Deutsche Forschungsgemeinschaft (DFG, German Research Foundation) under Germany's Excellence Strategy within the Cluster of Excellence PhoenixD (EXC 2122, Project ID 390833453) and the Cluster of Excellence QuantumFrontiers (EXC 2123, Project ID 390837967). The analysis of the bianisotropic coupling effects has been supported by the Russian Science Foundation Grant No. 20-12-00343. V.R.T. acknowledges financial support from the National Key R&D Program of China Project No. 2018YFE0119900.

-
- [1] N. I. Zheludev and Y. S. Kivshar, From metamaterials to metadevices, *Nat. Mater.* **11**, 917 (2012).
- [2] U. Zywiets, A. B. Evlyukhin, C. Reinhardt, and B. N. Chichkov, Laser printing of silicon nanoparticles with resonant optical electric and magnetic responses, *Nat. Commun.* **5**, 1 (2014).
- [3] D. G. Baranov, D. A. Zuev, S. I. Lepeshov, O. V. Kotov, A. E. Krasnok, A. B. Evlyukhin, and B. N. Chichkov, All-dielectric nanophotonics: The quest for better materials and fabrication techniques, *Optica* **4**, 814 (2017).
- [4] R. Won, Into the “Mie-tronic” era, *Nat. Photon.* **13**, 585 (2019).
- [5] S. Jahani and Z. Jacob, All-dielectric metamaterials, *Nat. Nanotechnol.* **11**, 23 (2016).
- [6] Z.-J. Yang, R. Jiang, X. Zhuo, Y.-M. Xie, J. Wang, and H.-Q. Lin, Dielectric nanoresonators for light manipulation, *Phys. Rep.* **701**, 1 (2017).
- [7] A. B. Evlyukhin, C. Reinhardt, A. Seidel, B. S. Luk'yanchuk, and B. N. Chichkov, Optical response features of Silicon nanoparticle arrays, *Phys. Rev. B* **82**, 045404 (2010).
- [8] A. García-Etxarri, R. Gómez-Medina, L. S. Froufe-Pérez, L. López, C. Chantada, F. Scheffold, J. Aizpurua, M. Nieto-Vesperinas, and J. J. Sáenz, Strong magnetic response of sub-micron silicon particles in the infrared, *Opt. Express* **19**, 4815 (2011).
- [9] P. D. Terekhov, K. V. Baryshnikova, Y. A. Artemyev, A. Karabchevsky, A. S. Shalin, and A. B. Evlyukhin, Multipolar response of nonspherical silicon nanoparticles in the visible and near-infrared spectral ranges, *Phys. Rev. B* **96**, 035443 (2017).
- [10] A. I. Kuznetsov, A. E. Miroshnichenko, M. L. Brongersma, Y. S. Kivshar, and B. Luk'yanchuk, Optically resonant dielectric nanostructures, *Science* **354**, aag2472 (2016).
- [11] A. B. Evlyukhin, S. M. Novikov, U. Zywiets, R. L. Eriksen, C. Reinhardt, S. I. Bozhevolnyi, and B. N. Chichkov, Demonstration of magnetic dipole resonances of dielectric nanospheres in the visible region, *Nano Lett.* **12**, 3749 (2012).
- [12] V. Khardikov, P. Mladyonov, S. Prosvirnin, and V. Tuz, Electromagnetic wave diffraction by periodic planar metamaterials with nonlinear constituents, in *Contemporary Optoelectronics: Materials, Metamaterials and Device Applications*, edited by O. Shulika and I. Sukhoivanov (Springer, Dordrecht, 2016), Chap. 5, pp. 81–98.
- [13] A. Krasnok, M. Tymchenko, and A. Alù, Nonlinear metasurfaces: A paradigm shift in nonlinear optics, *Mater. Today* **21**, 8 (2018).
- [14] G. Grinblat, Y. Li, M. P. Nielsen, R. F. Oulton, and S. A. Maier, Efficient third harmonic generation and nonlinear sub-wavelength imaging at a higher-order anapole mode in a single germanium nanodisk, *ACS Nano* **11**, 953 (2017).
- [15] K. Koshelev, S. Kruk, E. Melik-Gaykazyan, J.-H. Choi, A. Bogdanov, H.-G. Park, and Y. Kivshar, Subwavelength dielectric resonators for nonlinear nanophotonics, *Science* **367**, 288 (2020).
- [16] S. S. Kruk, R. Camacho-Morales, L. Xu, M. Rahmani, D. A. Smirnova, L. Wang, H. H. Tan, C. Jagadish, D. N. Neshev, and Y. S. Kivshar, Nonlinear optical magnetism revealed by second-harmonic generation in nanoantennas, *Nano Lett.* **17**, 3914 (2017).
- [17] J. Cambiasso, G. Grinblat, Y. Li, A. Rakovich, E. Cortés, and S. A. Maier, Bridging the gap between dielectric nanophotonics and the visible regime with effectively lossless gallium phosphide antennas, *Nano Lett.* **17**, 1219 (2017).
- [18] M. Celebrano, X. Wu, M. Baselli, S. Großmann, P. Biagioni, A. Locatelli, C. De Angelis, G. Cerullo, R. Osellame, B. Hecht, L. Duò, F. Ciccacci, and M. Finazzi, Mode matching in multi-resonant plasmonic nanoantennas for enhanced second harmonic generation, *Nat. Nanotechnol.* **10**, 412 (2015).
- [19] J. Butet, P.-F. Brevet, and O. J. F. Martin, Optical second harmonic generation in plasmonic nanostructures: From fundamental principles to advanced applications, *ACS Nano* **9**, 10545 (2015).

- [20] V. A. Fedotov, M. Rose, S. L. Prosvirnin, N. Papasimakis, and N. I. Zheludev, Sharp Trapped-Mode Resonances in Planar Metamaterials with a Broken Structural Symmetry, *Phys. Rev. Lett.* **99**, 147401 (2007).
- [21] V. V. Khardikov, E. O. Iarko, and S. L. Prosvirnin, A giant red shift and enhancement of the light confinement in a planar array of dielectric bars, *J. Opt.* **14**, 035103 (2012).
- [22] V. R. Tuz, V. V. Khardikov, A. S. Kupriianov, K. L. Domina, S. Xu, H. Wang, and H.-B. Sun, High-quality trapped modes in all-dielectric metamaterials, *Opt. Express* **26**, 2905 (2018).
- [23] P. Yu, A. S. Kupriianov, V. Dmitriev, and V. R. Tuz, All-dielectric metasurfaces with trapped modes: Group-theoretical description, *J. Appl. Phys.* **125**, 143101 (2019).
- [24] C. W. Hsu, B. Zhen, A. D. Stone, J. D. Joannopoulos, and M. Soljačić, Bound states in the continuum, *Nat. Rev. Mater.* **1**, 16048 (2016).
- [25] K. Koshelev, S. Lepeshov, M. Liu, A. Bogdanov, and Y. Kivshar, Asymmetric Metasurfaces with High- Q Resonances Governed by Bound States in the Continuum, *Phys. Rev. Lett.* **121**, 193903 (2018).
- [26] A. S. Kupriianov, Y. Xu, A. Sayanskiy, V. Dmitriev, Y. S. Kivshar, and V. R. Tuz, Metasurface Engineering through Bound States in the Continuum, *Phys. Rev. Appl.* **12**, 014024 (2019).
- [27] S. Li, C. Zhou, T. Liu, and S. Xiao, Symmetry-protected bound states in the continuum supported by all-dielectric metasurfaces, *Phys. Rev. A* **100**, 063803 (2019).
- [28] C. Cui, C. Zhou, S. Yuan, X. Qiu, L. Zhu, Y. Wang, Y. Li, J. Song, Q. Huang, Y. Wang, C. Zeng, and J. Xia, Multiple Fano resonances in symmetry-breaking silicon metasurface for manipulating light emission, *ACS Photon.* **5**, 4074 (2018).
- [29] G. Zhang, C. Lan, R. Gao, and J. Zhou, Trapped-mode-induced giant magnetic field enhancement in all-dielectric metasurfaces, *J. Phys. Chem. C* **123**, 28887 (2019).
- [30] L. Xu, K. Zangeneh Kamali, L. Huang, M. Rahmani, A. Smirnov, R. Camacho-Morales, Y. Ma, G. Zhang, M. Woolley, D. Neshev, and A. E. Miroshnichenko, Dynamic nonlinear image tuning through magnetic dipole quasi-BIC ultrathin resonators, *Adv. Sci.* **6**, 1802119 (2019).
- [31] K. Zangeneh Kamali, L. Xu, J. Ward, K. Wang, G. Li, A. E. Miroshnichenko, D. Neshev, and M. Rahmani, Reversible image contrast manipulation with thermally tunable dielectric metasurfaces, *Small* **15**, 1805142 (2019).
- [32] S. Zou and G. C. Schatz, Theoretical studies of plasmon resonances in one-dimensional nanoparticle chains: Narrow lineshapes with tunable widths, *Nanotechnol.* **17**, 2813 (2006).
- [33] V. A. Markel, Divergence of dipole sums and the nature of non-Lorentzian exponentially narrow resonances in one-dimensional periodic arrays of nanospheres, *J. Phys. B: At. Mol. Opt. Phys.* **38**, L115 (2005).
- [34] W. Liu, A. E. Miroshnichenko, D. N. Neshev, and Y. S. Kivshar, Polarization-independent Fano resonances in arrays of core-shell nanoparticles, *Phys. Rev. B* **86**, 081407(R) (2012).
- [35] A. D. Humphrey and W. L. Barnes, Plasmonic surface lattice resonances on arrays of different lattice symmetry, *Phys. Rev. B* **90**, 075404 (2014).
- [36] W. Zhou and T. W. Odom, Tunable subradiant lattice plasmons by out-of-plane dipolar interactions, *Nat. Nanotechnol.* **6**, 423 (2011).
- [37] V. G. Kravets, A. V. Kabashin, W. L. Barnes, and A. N. Grigorenko, Plasmonic surface lattice resonances: A review of properties and applications, *Chem. Rev.* **118**, 5912 (2018).
- [38] A. E. Miroshnichenko, S. Flach, and Y. S. Kivshar, Fano resonances in nanoscale structures, *Rev. Mod. Phys.* **82**, 2257 (2010).
- [39] G. W. Mulholland, C. F. Bohren, and K. A. Fuller, Light scattering by agglomerates: Coupled electric and magnetic dipole method, *Langmuir* **10**, 2533 (1994).
- [40] B. García-Cámara, F. Moreno, F. González, and O. J. F. Martin, Light scattering by an array of electric and magnetic nanoparticles, *Opt. Express* **18**, 10001 (2010).
- [41] V. S. Asadchy, I. A. Faniayev, Y. Ra'di, and S. A. Tretyakov, Determining polarizability tensors for an arbitrary small electromagnetic scatterer, *Photon. Nanostruct.: Fundam. Appl.* **12**, 298 (2014).
- [42] M. Yazdi and N. Komjani, Polarizability calculation of arbitrary individual scatterers, scatterers in arrays, and substrated scatterers, *J. Opt. Soc. Am. B* **33**, 491 (2016).
- [43] S. L. Prosvirnin, V. A. Dmitriev, Y. M. Kuleshov, and V. V. Khardikov, Planar all-silicon metamaterial for terahertz applications, *Appl. Opt.* **54**, 3986 (2015).
- [44] A. Jain, P. Moitra, T. Koschny, J. Valentine, and C. M. Soukoulis, Electric and magnetic response in dielectric dark states for low loss subwavelength optical meta atoms, *Adv. Opt. Mater.* **3**, 1431 (2015).
- [45] V. R. Tuz, V. V. Khardikov, and Y. S. Kivshar, All-dielectric resonant metasurfaces with a strong toroidal response, *ACS Photon.* **5**, 1871 (2018).
- [46] A. Sayanskiy, A. S. Kupriianov, S. Xu, P. Kapitanova, V. Dmitriev, V. V. Khardikov, and V. R. Tuz, Controlling high- Q trapped modes in polarization-insensitive all-dielectric metasurfaces, *Phys. Rev. B* **99**, 085306 (2019).
- [47] C. É. Kriegler, M. S. Rill, S. Linden, and M. Wegener, Bianisotropic photonic metamaterials, *IEEE J. Sel. Top. Quantum Electron.* **16**, 367 (2010).
- [48] R. Alae, M. Albooyeh, A. Rahimzadegan, M. S. Mirmoosa, Y. S. Kivshar, and C. Rockstuhl, All-dielectric reciprocal bianisotropic nanoparticles, *Phys. Rev. B* **92**, 245130 (2015).
- [49] M. Odit, P. Kapitanova, P. Belov, R. Alae, C. Rockstuhl, and Y. S. Kivshar, Experimental realisation of all-dielectric bianisotropic metasurfaces, *Appl. Phys. Lett.* **108**, 221903 (2016).
- [50] Z. Fan, M. R. Shcherbakov, M. Allen, J. Allen, B. Wenner, and G. Shvets, Perfect diffraction with multiresonant bianisotropic metagratings, *ACS Photon.* **5**, 4303 (2018).
- [51] V. S. Asadchy, A. Díaz-Rubio, and S. A. Tretyakov, Bianisotropic metasurfaces: Physics and applications, *Nanophotonics* **7**, 1069 (2018).
- [52] A. B. Evlyukhin, C. Reinhardt, and B. N. Chichkov, Multipole light scattering by nonspherical nanoparticles in the discrete dipole approximation, *Phys. Rev. B* **84**, 235429 (2011).
- [53] R. Alae, C. Rockstuhl, and I. Fernandez-Corbaton, An electromagnetic multipole expansion beyond the long-wavelength approximation, *Opt. Commun.* **407**, 17 (2018).
- [54] A. B. Evlyukhin and B. N. Chichkov, Multipole decompositions for directional light scattering, *Phys. Rev. B* **100**, 125415 (2019).
- [55] L. Onsager, Reciprocal relations in irreversible processes. I. *Phys. Rev.* **37**, 405 (1931).

- [56] L. Onsager, Reciprocal relations in irreversible processes. II. *Phys. Rev.* **38**, 2265 (1931).
- [57] H. B. G. Casimir, On Onsager's principle of microscopic reversibility, *Rev. Mod. Phys.* **17**, 343 (1945).
- [58] V. E. Babicheva and A. B. Evlyukhin, Analytical model of resonant electromagnetic dipole-quadrupole coupling in nanoparticle arrays, *Phys. Rev. B* **99**, 195444 (2019).
- [59] T. Niemi, A. O. Karilainen, and S. A. Tretyakov, Synthesis of polarization transformers, *IEEE Trans. Antennas Propag.* **61**, 3102 (2013).
- [60] R. Alaei, M. Albooyeh, M. Yazdi, N. Komjani, C. Simovski, F. Lederer, and C. Rockstuhl, Magnetolectric coupling in nonidentical plasmonic nanoparticles: Theory and applications, *Phys. Rev. B* **91**, 115119 (2015).
- [61] M. A. Yurkin and A. G. Hoekstra, The discrete dipole approximation: An overview and recent developments, *J. Quant. Spectrosc. Radiat. Transfer* **106**, 558 (2007).
- [62] B. T. Draine and P. J. Flatau, Discrete-dipole approximation for scattering calculations, *J. Opt. Soc. Am. A* **11**, 1491 (1994).
- [63] J. D. Jackson, *Classical Electrodynamics*, 3rd ed. (John Wiley & Sons, New York, 1999).
- [64] A. B. Evlyukhin, T. Fischer, C. Reinhardt, and B. N. Chichkov, Optical theorem and multipole scattering of light by arbitrarily shaped nanoparticles, *Phys. Rev. B* **94**, 205434 (2016).
- [65] A. N. Serdyukov, I. V. Semchenko, S. A. Tretyakov, and A. Sihvola, *Electromagnetics of Bi-anisotropic Materials: Theory and Application* (Gordon and Breach Science Publishers, Amsterdam, 2001).
- [66] V. E. Babicheva and A. B. Evlyukhin, Metasurfaces with electric quadrupole and magnetic dipole resonant coupling, *ACS Photon.* **5**, 2022 (2018).
- [67] A. Alù and N. Engheta, Theory of linear chains of metamaterial/plasmonic particles as subdiffraction optical nanotransmission lines, *Phys. Rev. B* **74**, 205436 (2006).
- [68] P. A. Belov, S. I. Maslovski, K. R. Simovski, and S. A. Tretyakov, A condition imposed on the electromagnetic polarizability of a bianisotropic lossless scatterer, *Tech. Phys. Lett.* **29**, 718 (2003).
- [69] I. Sersic, C. Tuambilangana, T. Kampfrath, and A. F. Koenderink, Magnetolectric point scattering theory for metamaterial scatterers, *Phys. Rev. B* **83**, 245102 (2011).
- [70] F. J. García de Abajo, Colloquium: Light scattering by particle and hole arrays, *Rev. Mod. Phys.* **79**, 1267 (2007).
- [71] J. Zhang, K. F. MacDonald, and N. I. Zheludev, Near-infrared trapped mode magnetic resonance in an all-dielectric metamaterial, *Opt. Express* **21**, 26721 (2013).
- [72] J. A. Burrow, R. Yahiaoui, A. Sarangan, I. Agha, J. Mathews, and T. A. Searles, Polarization-dependent electromagnetic responses of ultrathin and highly flexible asymmetric terahertz metasurfaces, *Opt. Express* **25**, 32540 (2017).
- [73] R. J. Potton, Reciprocity in optics, *Rep. Prog. Phys.* **67**, 717 (2004).